Published in final edited form as:
Atherosclerosis. 2012 October ; 224(2): 340–347. doi:10.1016/j.atherosclerosis.2012.07.023.

Detection of Hydroxyapatite in Calcified Cardiovascular Tissues

Jae Sam Lee[1], **Joel D. Morrisett**[2], and **Ching-Hsuan Tung**[1,*]

[1]Department of Radiology, The Methodist Hospital Research Institute, Weill Medical College of Cornell University, Houston, TX

[2]Department of Medicine, Atherosclerosis and Vascular Medicine Section, Methodist DeBakey Heart Center, Baylor College of Medicine, Houston, TX

Abstract

Objective—The objective of this study is to develop a method for selective detection of the calcific (hydroxyapatite) component in human aortic smooth muscle cells *in vitro* and in calcified cardiovascular tissues *ex vivo*. This method uses a novel optical molecular imaging contrast dye, Cy-HABP-19, to target calcified cells and tissues.

Methods—A peptide that mimics the binding affinity of osteocalcin was used to label hydroxyapatite *in vitro* and *ex vivo*. Morphological changes in vascular smooth muscle cells were evaluated at an early stage of the mineralization process induced by extrinsic stimuli, osteogenic factors and a magnetic suspension cell culture. Hydroxyapatite components were detected in monolayers of these cells in the presence of osteogenic factors and a magnetic suspension environment.

Results—Atherosclerotic plaque contains multiple components including lipidic, fibrotic, thrombotic, and calcific materials. Using optical imaging and the Cy-HABP-19 molecular imaging probe, we demonstrated that hydroxyapatite components could be selectively distinguished from various calcium salts in human aortic smooth muscle cells *in vitro* and in calcified cardiovascular tissues, carotid endarterectomy samples and aortic valves, *ex vivo*.

Conclusion—Hydroxyapatite deposits in cardiovascular tissues were selectively detected in the early stage of the calcification process using our Cy-HABP-19 probe. This new probe makes it possible to study the earliest events associated with vascular hydroxyapatite deposition at the cellular and molecular levels. This target-selective molecular imaging probe approach holds high potential for revealing early pathophysiological changes, leading to progression, regression, or stabilization of cardiovascular diseases.

Keywords

atherosclerosis; calcification; hydroxyapatite; molecular imaging; osteocalcin

*Correspondence to: Ching H. Tung, Department of Radiology, The Methodist Hospital Research Institute, 6565 Fannin Street, #B5-009, Houston, TX 77030. ctung@tmhs.org.

Conflict of Interests: None

Introduction

Cardiovascular calcification results in the deposition of insoluble calcium in tissues such as arteries, heart valves, and cardiac muscle[1, 2]. Arising from a systemic mineral imbalance, this physiological change is commonly observed in patients with cardiovascular disease (CVD)[3, 4]. Although the mechanism of vascular calcification is not fully understood, it has been suggested that vascular wall resident cells such as pericytes or vascular smooth muscle cells (VSMCs) may transdifferentiate and produce a mineralized matrix[5-7]. Accumulating evidence supports the hypothesis that most atherosclerosis-associated calcification results from highly regulated and organized active cellular processes[1, 2, 8-10]. It has been proposed that circulating osteoblast precursors or resident mesenchymal stem cells could produce ectopic calcification. However, it is more likely that calcifying vascular cells (CVCs), identified as a subpopulation of VSMCs, induce pathological calcification in response to environmental stimuli[7, 11]. CVCs secrete several osteogenic-associated proteins such as osteopontin, osteonectin, osteocalcin (OCN), bone sialoprotein (BSP), bone morphogenetic proteins (BMPs), and matrix Gla protein (MGP) into the extracellular matrix[11, 12]. Many of these proteins have a high binding affinity for calcium salts and accumulate in areas of vascular calcification, where they may play various roles including the regulation of calcium crystal nucleation and growth. In normal arterial walls, VSMCs constitutively express potent inhibitors of calcification, such as MGP, whose absence results in spontaneous calcification[1]. Understanding how these proteins regulate calcification is crucial for designing novel therapeutic approaches to treat calcification associated cardiovascular diseases.

The calcium deposits in cardiovascular tissues are comprised of various calcium salts, such as calcium carbonate (CC), calcium oxalate (CO), calcium phosphate (CP), calcium pyrophosphate (CPP), and Hydroxyapatite (HA). However, little information has been reported about these different forms of calcium salts in cardiovascular diseases. Even the most advanced clinical imaging modalities, such as optical coherence tomography, MRI, and ultrasonography have difficulty distinguishing them. Without a reliable analytical method, a clear correlation between various calcium salts and calcified vascular tissues cannot be obtained. Recently, we have developed a HA binding peptide (HABP-19), which can potentially be used as a tool to distinguish HA from other calcium salts in biological tissues. HABP-19 is a 19-residue peptide, derived from the bone-binding protein, OCN. Maturation of OCN requires posttranslational modifications, specifically vitamin K-dependent γ-carboxylation, resulting in the formation of three γ-carboxylated glutamic acid (Gla) residues from three glutamic acid (Glu) residues[13, 14]. The γ-carboxylated OCN is primarily associated with bone formation through its high binding affinity to HA, although a fraction is released into the circulation[15, 16]. In contrast, the under-carboxylated circulating form of OCN has been implicated as a novel hormone and positive regulator of glucose homeostasis[17, 18].

When labeled with a near-infrared (NIR) fluorochrome, the HABP-19 probe was able to disply HA in the skeletons of living animals for 6 weeks without significant signal reduction[19]. We hypothesized that this probe could distinguish HA from other calcium deposits in calcified cardiovascular tissues. In the present study, we have utilized fluorescently labeled HABP-19 to directly visualize the early-stage osteogenesis-like activity of VSMCs *in vitro*. We have also visualized HA calcification in CVD tissues, carotid endarterectomy tissues, and resected aortic valves *ex vivo*. This visualization of HA-dependent calcification is otherwise unidentifiable by conventional imaging modalities or routine histological methods.

Methods

Fluorescein isothiocyanate (FITC) labeled HABP-19, Cy5.5 labeled Cy-HABP-19, and the corresponding FITC-labeled control cHABP probes (Table 1) were synthesized as previously reported[19]. FITC dye (Sigma-Aldrich) was also included as a negative control dye.

Binding kinetics of various calcium salts and HABPs

The binding affinities of FITC, cHABP, and HABP-19 to HA was evaluated by incubating 1 ml of 10 μM peptide solution with 10 mg HA ($Ca_5(PO_4)_3OH$; Sigma, St. Louis, MO) at room temperature (RT) for 3 h with constant agitation. The amount of peptide in solution bound to HA was determined indirectly by measuring unbound peptide in solution (490 nm) using a SpectraMax M2 Microplate (Molecular Devices, Sunnyvale, CA) and comparing these values those of the FITC standard in PBS buffer (pH = 7.2) at 490 nm (ε = 67,000). To further characterize the binding affinity of HABP-19 to calcium carbonate ($CaCO_3$; Sigma), calcium oxalate ($Ca(CO_2)_2.H_2O$; Fisher Scientific, Waltham, MA), calcium phosphate ($Ca_3(PO_4)_2$; Fisher Scientific), or calcium pyrophosphate ($Ca_2P_2O_7$; Sigma), HABP-19 was incubated separately with each calcium salt for 3 h at RT. The amount of HABP-19 bound to each calcium salt was determined indirectly by measuring unbound HABP-19 in solution as aforementioned.

Cell culture and induction of mineralization

Human aortic vascular smooth muscle cells (VSMCs; 1.5×10^4 per cm^2) (Genlantis, San Diego, CA) were grown in 35 mm^2 petri dishes supplemented with 2 ml of smooth muscle cell growth medium (SMCGM; Genlantis) in triplicate. Mineralization was induced by culturing the cells in SMCGM as the control medium, or SMCGM supplemented with 50 μg/ml ascorbic acid (AA), 7.5 mM β-glycerophosphate (β-GP), and 10 nM l-α-lyso-phosphatidylcholine (LPC; Type I, 99%, Sigma) as the stimulating medium. In order to provide *in vitro* magnetic stimuli to VSMCs, cells grown to 80% confluence in T-175 flasks were transferred to 35 mm^2 petri dishes and treated with Nanoshuttle-PL™ (Ns), a polylysine based hydrogel containing gold and magnetite nanoparticles (n3D Biosciences, Houston, TX), for 8h. After the cells had taken up the Ns, they were magnetically levitated using a magnetic drive (n3D Biosciences) and cultured for 4 days in control or stimulating media (*in vitro* magnetic suspension). The first day of culture in stimulating media for the induction of mineralization was defined as day 0. The culture medium was replaced with fresh medium every 2 days.

Quantification of mineralized layers by Alizarin Red S (ARS) staining

Quantification of mineralized tissue formation was performed as previously described[20, 21]. In brief, the magnetic drive was removed from the top of each dish to allow the cell suspensions in the 3D cultures to settle and spread at the bottom for 4 h. The resultant cell monolayer was washed with PBS, fixed in formalin, and incubated with ARS (pH 4.2). To quantify ARS staining, the monolayer was incubated in 400 l of 10% (v/v) acetic acid, scraped from the plate, and transferred to a 1.5-ml tube. The mixture was overlaid with mineral oil, heated to exactly 85 °C, centrifuged, and 300 μl of the supernatant was transferred to a new 1.5-ml tube. 200 l of 10% (v/v) ammonium hydroxide was added to neutralize the acid. The absorbance of the aliquots was measured in triplicate at 405 nm in a 96-well plate.

Fluorescence microscopy

Each cell monolayer was washed with PBS and stained with 2 nmol of FITC, cHABP, or HABP-19 at RT for 60 min. The monolayer was then washed extensively with PBS to remove unincorporated probes. Fluorescence images were captured using an IX51 microscope (Olympus, Center Valley, PA) with excitation at 488 nm (FITC-tagged LP). FV 1000 Viewer software (Olympus) was used for image analysis

Tissue acquisition and storage

Carotid endarterectomy and aortic valve specimens were acquired within 1 h after surgical resection and stored until use in 50% glycerol/PBS (4°C) to prese rve tissue morphology. The use of the specimens was approved by the institutional review board (IRB) of Baylor College of Medicine (Houston, TX).

Histology

Human aortic valves were fixed in 10% formalin, dehydrated in a graded series of ethanol washes, and embedded in glycomethylmethacrylate. After polymerization, thin sections (5 μm) were prepared using the Exakt System modified sawing microtome technique[22]. Serial sections were stained with a Von Kossa reagent (American MasterTech, Lodi, CA) or with molecular imaging probes (HABPs).

Optical imaging acquisition

For *ex vivo* optical imaging, each specimen was incubated with 2 nmol of FITC, cHABP, HABP-19, or Cy-HABP-19 for 1 h with constant agitation, thoroughly washed with PBS to remove unbound probe, resuspended into PBS solution, and images were acquired using the Maestro 2 optical imaging system (CRI, Woburn, MA). To validate the selective accumulation of imaging probes, a green (FITC) filter set (acquisition setting: 550 to 800 in 10 nm steps and 10 ms exposure time) was used for FITC, cHABP, and HABP-19. A red (CY5.5) filter set (acquisition setting: 680 to 950 in 10 nm steps and 10 ms exposure time) was utilized for Cy-HABP-19. The fluorescence images obtained were corrected to remove the auto-fluorescence background using the multi-excitation spectral analysis function (Maestro software v. 2.10).

Micro computed tomography (μCT) analysis

Micro CT was performed using a Siemens Inveon Preclinical Multimodel PET/SPECT/CT system (Malvern, PA) at medium resolution. Real-time images were reconstructed for correlation with the optical imaging system. An internal infrared video camera allows visual sample monitoring during scan acquisition. The scanner was operated in the 3 D volume imaging acquisition mode. Specimens were laser aligned at the center of the field of view of the scanner for subsequent imaging. The μCT image was acquired in approximately 3 min, and concurrent image reconstruction was achieved using a COBRA (Siemens). Invenon Research Workplace software (Siemens) was used to view and adjust imaging.

Statistical analysis

In vitro and *ex vivo* data were analyzed for statistical significance by the Student's t-test or one way ANOVA and Dunnett post hoc test, using the Statistical Package for the Social Sciences (SPSS) software, version 13 (SPSS, Chicago, IL). Means, standard deviations, and degrees of significance are shown on individual data graphs in the 'Results' section. A probability value (P) of < 0.05 was considered statistically significant unless otherwise indicated.

Results

The HABP-19 probe specifically recognizes HA salt

The HA specificity of the prepared probes was determined by incubating HA with FITC, cHABP, and HABP-19 solutions for 3 h. The HA binding affinity of each probe was quantified by measuring the absorbance of solution (490 nm) (Figure 1). HABP-19, which has 6 Gla residues, exhibited a rather high HA binding affinity (86.2 ± 4.1 %), whereas neither cHABP (3.3 ± 3.2 %) nor control FITC (4.2 ± 2.2 %) showed appreciable HA binding ($P < 0.005$), suggesting a crucial role for the Gla residues within HABP-19 for binding to HA, as previously reported[19-21]. To confirm the HA binding specificity of HABP-19, a panel of calcium salts, CC, CO, CP, CPP and HA, were incubated in HABP-19 solutions. HABP-19 exhibited exceptional binding affinity for HA but not for the other calcium salts ($P < 0.005$). Our data indicate that HABP-19 has 25-fold higher binding affinity for HA than does cHABP, and >6-fold higher specificity for HA than the other calcium salts tested (Figure 1).

Induction of calcification in human aortic smooth muscle cells

To study the early stages of the mineralization process in VSMCs, cells were cultured in control media (CM) or stimulating media (SM) supplemented with AA, β-GP, and LPC. AA and β-GP are known osteogenic factors that stimulate osteoblastic differentiation and mineralization[23-25]. LPC, a product of oxidized phosphatidylcholine hydrolysis, is a candidate compound thought to act on VSMCs and stimulate their transition into calcifying vascular cells, and it likely plays a significant role in the calcification of atherosclerotic plaques[7]. In a normal 2D culture, VSMCs cultured in SM grew into a dense monolayer in 3 days, whereas VSMCs grown in CM were smaller and less organized (Figure 2A and Figure I in the online-only Data Supplement). Cells treated with Nanoshuttle (Ns), without applying the magnetic field, exhibited elongated spindle-like cell shapes and formed nodules with pronounced dark ridges, reflecting the presence of iron nanoparticles (Figure 2B). However, Ns treated and magnetically levitated VSMCs were capable of forming large cell clusters in the central region beneath the circular magnet drive at day 3 (Figure 2C). Diffusely scattered spherical clusters of cells were also observed.

To validate the difference in mineralization, the treated cells were stained with ARS and quantified by absorbance spectroscopy (Figure 2D and 2E). Cells cultured in 3D-Ns SM promoted the most mineral deposition. ARS measurements showed that the enhancement was more than 5-fold higher than in normal 2D cultures ($P = 0.0204$) (Figure 2E). However, the effect of CM and SM in all three study groups was not statistically significant. Hence the effects of extrinsic osteogenic factors in influencing the biological activity of VSMCs in these early time points.

Identifying HA calcification in human aortic smooth muscle cells by HABP-19

Based on the above ARS mineralization results, 3D-Ns cultured VSMCs cells were selected for HABP-19 binding studies. Four days after stimulation, HA deposition was monitored after staining with HABP-19 and controls. As expected, a large fluorescence signal was seen in the HABP-19 stained cells, whereas minimal signal was observed in either the cHABP or FITC stained cells (Figure 3). Other culture conditions (2D and 2D-Ns cultures) did not result in the deposition of a significant amount of HA (Figures II and III in the online-only Data Supplement).

Detecting HA deposition in excised calcified human aortic valves

The potential detection of HA in biological tissues was then tested with human specimens. Calcified human aortic valves resected during valve replacement procedures were sliced into

four pieces. The degree of calcification of these pieces was confirmed by μCT which is routinely used to visualize bones and calcified tissues[26]. The obtained 2D and 3D CT images indicate various degrees of calcification in these specimens (Figure 4C and Movie I in the online-only Data Supplement). A characteristic pattern of mineralization was observed. Calcium depositions were mostly oriented toward the center cusp area of the aortic valves. Although the CT images revealed the area of calcification, they did not allow for differentiation of HA from other calcium components. The bright field image and fluorescence image of an aortic valve before incubation with probes are shown in Figure 4A and 4B, respectively. The selective HA binding affinity of HABP-19 was then investigated by incubating the spliced specimens in PBS, FITC, cHABP, or HABP-19 for 1 h and removing the unbound probes (Figure 4D-4F). Fluorescence imaging showed a bright HAPB-19-dependent signal. Minimal signal was observed with cHABP. Although a non-specific background signal was initially observed with FITC, it quickly decreased with time. Nevertheless, a strong HABP-19 signal was sustained throughout. Optical molecular images of calcified aortic valves treated with the HABP-19 probe exhibited intense HA accumulation at calcified regions, as indicated by an arrowhead (Figure 4C and 4F).

Histological analysis of calcified human aortic valves

Histological analysis of the calcified plaque was performed to determine HA distribution at the tissue level. It is known that calcium salts in paraffin-embedded tissues can be lost during the sectioning process. Thus the aortic valve tissue here was embedded in plastic to avoid this complication (Figure 5). Consecutively sectioned aortic valves (Figure 5A) were stained with Von Kossa reagent commonly used to visualize calcium salts in histological tissues (Figure 5B); molecular imaging probes, including FITC dye, cHABP, and HABP-19 (Figure 5C). Dark Von Kossa-dependent staining exhibited dense calcification in a band-like pattern (Figure 5B). However, staining of consecutive sections using HABP-19 revealed a more restricted pattern of HA deposition within the medial part (delineated by red lines in Figure 5C). Aortic valves stained with FITC dye or cHABP did not exhibit detectable fluorescence. The HABP-19 and Von Kossa staining patterns were different in terms of their binding selectivity. The Von Kossa reagent stained all calcium salts, regardless of their phosphate content, while HABP-19 stain was selective for HA deposits.

Visualization of HA deposition in calcified cardiovascular specimens by the NIR HABP-19 probe

HA deposition in calcified cardiovascular tissues was further visualized using the NIR dye labeled Cy-HABP-19 imaging probe. This probe has increased sensitivity for real-time imaging and may provide non-invasive optical detection of HA deposition in cardiovascular tissues[27]. Surgically excised human carotid atheroma specimens and aortic valves were incubated with Cy-HABP-19 for 1 h, and unbound probes were removed by washing with water. Images of calcified cardiovascular tissues were obtained and analyzed by an optical imaging system and μCT (Figure 6). Digital images of carotid atheroma specimens (Figure 6A) and aortic valves (Figure 6B) clearly show an intense Cy-HABP-19-dependent signal within the calcified regions, primarily within tissue areas surrounding the bifurcation of carotid tissues and within the cusp area of aortic valves. μCT images showed large areas of calcium deposits (white) on the tissues (Figure 6C-D), whereas NIR optical images facilitated distinct detection of HA on the calcified cardiovascular tissues (Figure 6E-F). Background fluorescence signals induced by non-specific binding or auto-fluorescence in the aortic valves were not detectable in the NIR image; the tissue is therefore outlined with a dotted line (Figure 6E). Although Cy-HABP-19 deposits matched the calcified regions seen on the CT images, there was a disparity between two imaging modalities with respect to selectivity. Cy-HABP-19 with NIR optical imaging was able to differentiate HA calcification from other components.

Discussion

There is considerable interest in furthering our understanding of the mechanisms of cardiovascular calcification and its implications in CVD[3, 4]. ENREF_2 Calcium salts of different forms are generated by locally produced stimuli; however, little is known regarding the correlation between the type and composition of the calcium salt, and tissue changes. In calcified vascular tissues, two distinct calcium compounds have been identified based on their chemical composition, CO ($CaC_2O_4 \cdot 2H_2O$) and HA ($Ca_{10}(PO_4) \cdot 6H_2O$). It has been reported that calcium deposits seen in arteries and cartilage are mainly composed of HA, as seen in bone[1]. In this study, we describe a specific and sensitive tool to study HA, one of the main types of biological calcium deposits.

Previously, we developed fluorescence conjugated HA binding peptides (HABPs) inspired by the protein OCN; these peptides mimic natural OCN-HA binding properties by forming α-helices with HA in the skeleton of live animals[19]. Because bone mineralization and vascular calcification share a similar mechanism, our prior findings could be applied to detect HA calcification associated with cardiovascular diseases. We hypothesized that a HABP-19 probe could selectively detect HA calcification and may help predict potential risks for clinical complications in patients with CVD. The HA binding specificity of the HABP-19 probe was demonstrated using pure calcium salts, stimulated cell culture, and surgically excised specimens. Upon incubation with different types of salts, HABP-19 showed selective HA binding compared to cHABP and FITC (negative control dye, Figure 1). Substitution of the critical Gla residues with Glu amino acids in cHABP resulted in a complete loss of its HA binding capability, indicating that the Gla residues within the HABP-19 probe are responsible for HA binding specificity[16, 19-21, 28]. The HA-binding selectivity was further tested by incubating HABP-19 with different forms of calcium salts. The fluorescent signal resulting from incubation of HABP-19 with HA salt was significantly higher than that resulting from all other salts, confirming the binding specificity of HABP-19 for HA.

It has been shown that VSMCs grown in the presence of osteogenic factors, such as AA, β-GP, and LPC, exhibit extensive matrix mineralization with minerals such as HA, calcifying collagen, extracellular matrix vesicles, and nodular calcification, similar to that observed in calcified atherosclerotic plaques and heart valves *in vivo*[29]. Thus, we evaluated whether HA deposition is present in the matrix monolayer during the early stage of VSMC mineralization *in vitro*. VSMCs were cultured with extrinsic stimuli, including osteogenic inducible factors, and in a 3D microenvironment. ARS analysis illustrated that mineral formation in VSMCs cultures was more dependent upon the 3D environment than on extrinsic factors (Figure 2D). Following incubation with the fluorescent HABP-19 molecular imaging probe, fluorescence microscopy revealed that HA deposits were found on the mineral layer of both magnetically levitated 3D (Ns) VSMCs and VSMCs cultured in the presence of osteogenic factors under fluorescence microscopy. Neither 3D culture nor osteogenic factors alone promoted detectable HA calcification *in vitro* (Figures II and III in the online-only Data Supplement). As expected, other control probes were unable to bind HA. Our data suggest that 3D stimuli were much more effective in inducing HA calcification of VSMCs than were extrinsic osteogenic factors, and importantly, that HABP-19 is capable of detecting newly formed HA.

Ectopic calcification has a detrimental effect on vascular function and is associated with increased mortality in cardiovascular diseases, type 2 diabetes, and chronic kidney disease[30]. The majority of ruptured plaques contain HA deposits[2, 8-10]; therefore, HA deposition might be a good indicator of plaque vulnerability. Although early diagnosis is crucial for identifying vascular plaques induced by ectopic calcification before symptoms develop,

there is no stable, selective, and sensitive indicator to detect plaques associated with HA, or to distinguish HA from other calcium salts without the possibility of negative feedback. Therefore, we examined the potential of HABP-19 to distinguish HA from other types of calcium deposits in calcified human aortic valves that were collected after valve replacement. General calcification was first surveyed by μCT. These μCT images confirmed that these patient tissues were highly calcified. In contrast to the large calcified areas identified by μCT, only small regions among the μCT highlighted areas was highlighted by HABP-19, presumably the HA rich regions. These differences suggest that not all calcium deposits on the aortic valves has the same composition. Previously, Ortlepp et al. have determined HA composition from the excised aortic valves[31]. Calcium contents were initially determined by atomic absorption analysis, and, according to the X-ray diffraction (XRD) measurements, the calcification in the valves was concluded to be calcium-deficient HA, $Ca_{10-x}(HPO_4)_x(PO_4)_{6-x}(OH)_{2-x}$, with $0 \leq x \leq 1$, suggesting that HA was mixed with other calcified deposits. Since the detail chemical information of calcium deposits in tissues is largely under-studied, this HABP-19 imaging probe might be useful in distinguishing HA rich depositions from other mineral components. Detail composition of the calcified atherosclerotic plaques could be analyzed by various SEM/XRD spectroscopies[32-34].

We further conducted histological analyses to identify calcium salts and their distribution in the sectioned tissues by comparing Von Kossa staining with staining using our molecular imaging probe. Although routine histological methods are useful for visualizing calcification of cardiovascular tissues, the sectioning process itself often results in a loss of calcium crystals. Thus, a plastic embedding process was introduced in the present study to minimize calcium salt loss during sectioning. Calcification staining results showed that the Von Kossa assay stained entire mineralized layers and lacked adequate specificity. Conversely, fluorescence images using our HABP-19 probe clearly indicated a restricted stained area, mainly corresponding to HA deposits that were not selectively detected by Von Kossa staining (Figure 5).

For *in vivo* HA imaging, NIR fluorescence (NIRF) molecular imaging offers several advantages, including relatively deep photon penetration into tissue and reduced auto-fluorescence[27, 35]. NIR conjugated Cy-HABP-19 optical images exhibited distinct HA-detecting capability at the surface of calcified cardiovascular tissues compared to μCT images or fluorescence imaging acquired with visible light (Figure 4 vs. Figure 6). Therefore, Cy-HABP-19 could potentially be used as a unique molecular imaging probe offering previously unavailable information on HA deposition, and detecting early stage cardiovascular disease. The distinct HA selectivity of this probe may be especially useful in studies of older individuals, in which HA deposition may have occurred, but the calcification being imaged is the result of deposition of non-HA calcium salts[27]. ENREF_27 A bisphosphonate-based imaging contrast agent has previously been developed to image osteogenic activity in atherosclerotic plaques in mice models[27, 36, 37]. Our results indicate that HABP-19 could be applied to detect HA deposition in human tissues and, potentially, within patients, thereby offering a new diagnostic tool to assess clinical risk and monitor the efficacy of various interventions[37, 38]. However, the optical technology is not suitable for whole body imaging. Other imaging reporters, such as PET, SPECT, or MRI tracers, could be tethered to Cy-HABP-19 for whole-body multi-functional imaging.

Although the contribution of atherosclerotic calcification to plaque rupture is undefined, previous studies have revealed that inflammation precedes calcification in early-stage atherosclerosis, suggesting that macrophages promote the proinflammatory environment and send specific signals to vascular wall cells to initiate osteogenic differentiation[37, 39]. Subsequently, both inflammation and calcification processes developed in parallel and

within close proximity. The microcalcification stage may cause plaque rupture and microfractures that may results in the acute clinical events[40]. Once equilibrium in the artery shifts toward calcification, HA deposition could quickly advance and drive disease progression[37]. Virmani et. al. have demonstrated that a specific type of lesion with a calcified nodule is prone to rupture; these lesions consist of a fibrous cap disrupted by dense calcific nodules[41-43]. They hypothesize that these plaques may rupture owing to physical stress exerted by the nodules. On the other hand, other evidence indicates that calcified plaque may be more stable and, thus, less prone to rupture than noncalcified lesions[44]. In summary, the contribution of calcification to plaque vulnerability remains controversial and further investigation is required. The developed HABP-19 could represent a useful tool for further investigation of the mechanisms of vascular calcification, in particular HA formation.

Supplementary Material

Refer to Web version on PubMed Central for supplementary material.

Acknowledgments

This research was supported in part by NIH CA135312 and HL63090. The authors would like to thank Dr. Xukui Wang for μCT imaging and Dr. Glauco R. Souza for technical consultation of 3D Nanoshuttle cell culturing system (n3D Biosciences, Inc.).

References

[1]. Luo G, Ducy P, McKee MD, et al. Spontaneous calcification of arteries and cartilage in mice lacking matrix GLA protein. Nature. 1997; 386:78–81. [PubMed: 9052783]

[2]. Jono S, McKee MD, Murry CE, et al. Phosphate regulation of vascular smooth muscle cell calcification. Circ Res. 2000; 87:E10–17. [PubMed: 11009570]

[3]. Lusis AJ. Atherosclerosis. Nature. 2000; 407:233–241. [PubMed: 11001066]

[4]. Higgins CL, Marvel SA, Morrisett JD. Quantification of calcification in atherosclerotic lesions. Arterioscler Thromb Vasc Biol. 2005; 25:1567–1576. [PubMed: 15920031]

[5]. Iyemere VP, Proudfoot D, Weissberg PL, et al. Vascular smooth muscle cell phenotypic plasticity and the regulation of vascular calcification. J Intern Med. 2006; 260:192–210. [PubMed: 16918817]

[6]. Collett GD, Canfield AE. Angiogenesis and pericytes in the initiation of ectopic calcification. Circ Res. 2005; 96:930–938. [PubMed: 15890980]

[7]. Vickers KC, Castro-Chavez F, Morrisett JD. Lyso-phosphatidylcholine induces osteogenic gene expression and phenotype in vascular smooth muscle cells. Atherosclerosis. 2010; 211:122–129. [PubMed: 20451909]

[8]. Doherty TM, Asotra K, Fitzpatrick LA, et al. Calcification in atherosclerosis: bone biology and chronic inflammation at the arterial crossroads. Proc Natl Acad Sci U S A. 2003; 100:11201–11206. [PubMed: 14500910]

[9]. Johnson RC, Leopold JA, Loscalzo J. Vascular calcification: pathobiological mechanisms and clinical implications. Circ Res. 2006; 99:1044–1059. [PubMed: 17095733]

[10]. Shroff RC, Shanahan CM. The vascular biology of calcification. Semin Dial. 2007; 20:103–109. [PubMed: 17374082]

[11]. Vattikuti R, Towler DA. Osteogenic regulation of vascular calcification: an early perspective. Am J Physiol Endocrinol Metab. 2004; 286:E686–696. [PubMed: 15102615]

[12]. Tyson KL, Reynolds JL, McNair R, et al. Osteo/chondrocytic transcription factors and their target genes exhibit distinct patterns of expression in human arterial calcification. Arterioscler Thromb Vasc Biol. 2003; 23:489–494. [PubMed: 12615658]

[13]. Hauschka PV, Carr SA. Calcium-dependent alpha-helical structure in osteocalcin. Biochemistry. 1982; 21:2538–2547. [PubMed: 6807342]

[14]. Kelleher NL, Zubarev RA, Bush K, et al. Localization of labile posttranslational modifications by electron capture dissociation: the case of gamma-carboxyglutamic acid. Anal Chem. 1999; 71:4250–4253. [PubMed: 10517147]

[15]. Ducy P, Desbois C, Boyce B, et al. Increased bone formation in osteocalcin-deficient mice. Nature. 1996; 382:448–452. [PubMed: 8684484]

[16]. Hoang QQ, Sicheri F, Howard AJ, et al. Bone recognition mechanism of porcine osteocalcin from crystal structure. Nature. 2003; 425:977–980. [PubMed: 14586470]

[17]. Lee NK, Sowa H, Hinoi E, et al. Endocrine regulation of energy metabolism by the skeleton. Cell. 2007; 130:456–469. [PubMed: 17693256]

[18]. Ferron M, Wei J, Yoshizawa T, et al. Insulin signaling in osteoblasts integrates bone remodeling and energy metabolism. Cell. 2010; 142:296–308. [PubMed: 20655470]

[19]. Lee JS, Tung CH. Osteocalcin biomimic recognizes bone hydroxyapatite. ChemBioChem. 2011; 12:1669–1673. [PubMed: 21661088]

[20]. Lee JS, Lee JS, Wagoner-Johnson A, et al. Modular peptide growth factors for substrate-mediated stem cell differentiation. Angew Chem Int Ed Engl. 2009; 48:6266–6269. [PubMed: 19610001]

[21]. Lee JS, Lee JS, Murphy WL. Modular peptides promote human mesenchymal stem cell differentiation on biomaterial surfaces. Acta Biomater. 2010; 6:21–28. [PubMed: 19665062]

[22]. Kieffer P, Robert A, Capdeville-Atkinson C, et al. Age-related arterial calcification in rats. Life Sci. 2000; 66:2371–2381. [PubMed: 10864099]

[23]. Gillette JM, Nielsen-Preiss SM. The role of annexin 2 in osteoblastic mineralization. J Cell Sci. 2004; 117:441–449. [PubMed: 14679310]

[24]. Vaingankar SM, Fitzpatrick TA, Johnson K, et al. Subcellular targeting and function of osteoblast nucleotide pyrophosphatase phosphodiesterase 1. Am J Physiol Cell Physiol. 2004; 286:C1177–1187. [PubMed: 15075217]

[25]. Thouverey C, Strzelecka-Kiliszek A, Balcerzak M, et al. Matrix vesicles originate from apical membrane microvilli of mineralizing osteoblast-like Saos-2 cells. J Cell Biochem. 2009; 106:127–138. [PubMed: 19009559]

[26]. Waarsing JH, Day JS, van der Linden JC, et al. Detecting and tracking local changes in the tibiae of individual rats: a novel method to analyse longitudinal in vivo micro-CT data. Bone. 2004; 34:163–169. [PubMed: 14751574]

[27]. Zaheer A, Murshed M, De Grand AM, et al. Optical imaging of hydroxyapatite in the calcified vasculature of transgenic animals. Arterioscler Thromb Vasc Biol. 2006; 26:1132–1136. [PubMed: 16484598]

[28]. Capriotti LA, Beebe TP Jr. Schneider JP. Hydroxyapatite surface-induced peptide folding. J. Am. Chem. Soc. 2007; 129:5281–5287. [PubMed: 17397165]

[29]. Steitz SA, Speer MY, Curinga G, et al. Smooth muscle cell phenotypic transition associated with calcification: upregulation of Cbfa1 and downregulation of smooth muscle lineage markers. Circ Res. 2001; 89:1147–1154. [PubMed: 11739279]

[30]. Sage AP, Tintut Y, Demer LL. Regulatory mechanisms in vascular calcification. Nat Rev Cardiol. 2010; 7:528–536. [PubMed: 20664518]

[31]. Ortlepp JR, Schmitz F, Mevissen V, et al. The amount of calcium-deficient hexagonal hydroxyapatite in aortic valves is influenced by gender and associated with genetic polymorphisms in patients with severe calcific aortic stenosis. Eur Heart J. 2004; 25:514–522. [PubMed: 15039132]

[32]. Duer MJ, Friscic T, Proudfoot D, et al. Mineral surface in calcified plaque is like that of bone: further evidence for regulated mineralization. Arterioscler Thromb Vasc Biol. 2008; 28:2030–2034. [PubMed: 18703777]

[33]. Mikroulis D, Mavrilas D, Kapolos J, et al. Physicochemical and microscopical study of calcific deposits from natural and bioprosthetic heart valves. Comparison and implications for mineralization mechanism. J Mater Sci Mater Med. 2002; 13:885–889. [PubMed: 15348554]

[34]. Delogne C, Lawford PV, Habesch SM, et al. Characterization of the calcification of cardiac valve bioprostheses by environmental scanning electron microscopy and vibrational spectroscopy. J Microsc. 2007; 228:62–77. [PubMed: 17910699]

[35]. Jaffer FA, Libby P, Weissleder R. Optical and multimodality molecular imaging: insights into atherosclerosis. Arterioscler Thromb Vasc Biol. 2009; 29:1017–1024. [PubMed: 19359659]

[36]. Zaheer A, Lenkinski RE, Mahmood A, et al. In vivo near-infrared fluorescence imaging of osteoblastic activity. Nat Biotechnol. 2001; 19:1148–1154. [PubMed: 11731784]

[37]. Aikawa E, Nahrendorf M, Figueiredo JL, et al. Osteogenesis associates with inflammation in early-stage atherosclerosis evaluated by molecular imaging in vivo. Circulation. 2007; 116:2841–2850. [PubMed: 18040026]

[38]. Aikawa E, Nahrendorf M, Sosnovik D, et al. Multimodality molecular imaging identifies proteolytic and osteogenic activities in early aortic valve disease. Circulation. 2007; 115:377–386. [PubMed: 17224478]

[39]. Rattazzi M, Bennett BJ, Bea F, et al. Calcification of advanced atherosclerotic lesions in the innominate arteries of ApoE-deficient mice: potential role of chondrocyte-like cells. Arterioscler Thromb Vasc Biol. 2005; 25:1420–1425. [PubMed: 15845913]

[40]. Vengrenyuk Y, Carlier S, Xanthos S, et al. A hypothesis for vulnerable plaque rupture due to stress-induced debonding around cellular microcalcifications in thin fibrous caps. Proc Natl Acad Sci U S A. 2006; 103:14678–14683. [PubMed: 17003118]

[41]. Virmani R, Burke AP, Farb A. Plaque morphology in sudden coronary death. Cardiologia. 1998; 43:267–271. [PubMed: 9611854]

[42]. Virmani R, Kolodgie FD, Burke AP, et al. Lessons from sudden coronary death: a comprehensive morphological classification scheme for atherosclerotic lesions. Arterioscler Thromb Vasc Biol. 2000; 20:1262–1275. [PubMed: 10807742]

[43]. Virmani R, Burke AP, Kolodgie FD, et al. Pathology of the thin-cap fibroatheroma: a type of vulnerable plaque. J Interv Cardiol. 2003; 16:267–272. [PubMed: 12800406]

[44]. Nandalur KR, Baskurt E, Hagspiel KD, et al. Calcified carotid atherosclerotic plaque is associated less with ischemic symptoms than is noncalcified plaque on MDCT. AJR Am J Roentgenol. 2005; 184:295–298. [PubMed: 15615991]

Highlights

- Distinguish hydroxyapatite from other calcium salts in cardiovascular tissues
- A novel optical molecular imaging probe to target calcified cells and tissues
- Study the early events associated with vascular hydroxyapatite deposition
- Advantage of 3D culture in calcification

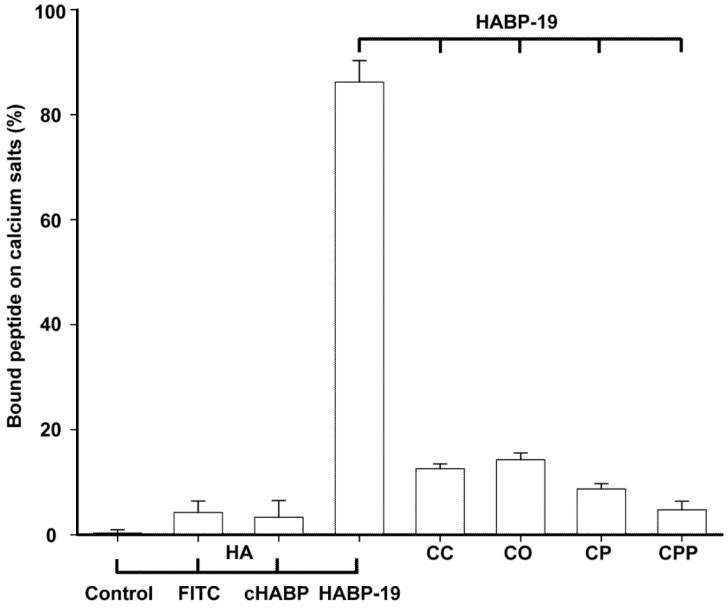

Figure 1.

Hydroxyapatite (HA) specificity of HABP-19. HA (5 mg) was incubated in 10 μM of FITC dye, cHABP, or HABP-19 solution at room temperature for 3 h with constant stirring. Several calcium salts (5 mg each) were also incubated with HABP-19 (10 μM) individually under the same conditions. The tested calcium salts were calcium carbonate (CC), calcium oxalate (CO), calcium phosphate (CP), calcium pyrophosphate (CPP), and HA. Quantification of the amount of imaging probe bound to HA, and of HABP-19 bound to calcium salts, was determined as described in the Methods section.

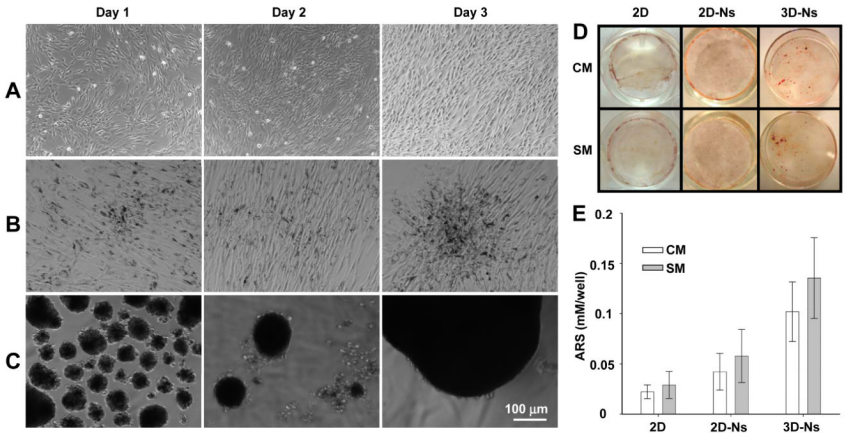

Figure 2.

Morphological changes and mineralization of VSMCs. Cells were incubated in control media (CM), or in stimulating media (SM) supplemented with 50 μg/ml ascorbic acid (AA), 7.5 mM β-glycerophosphate (β-GP), and 10 nM l-α-lyso-phosphatidylcholine (LPC) for 4 days. Morphology of VSMCs in 2D (A), 2D-Ns (B), or 3D-Ns (C) SM cultures. Cells were washed with PBS and observed under light microscopy. Images of cells cultured in CM are shown in Supplemental Figure II. (D) Cells cultured in CM or SM were stained with Alizarin Red-S (ARS) to detect the calcium mineral layer and images captured by a digital camera after the removal of unbound ARS dye by washing with water. (E) Mineral layers stained with ARS in CM or SM were quantified at 405 nm (results are mean ± SD, n = 4).

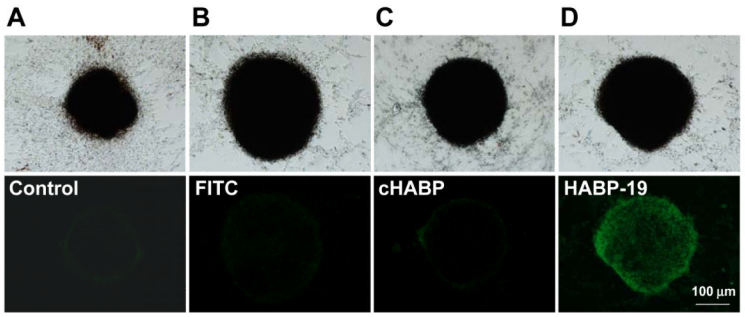

Figure 3.

Images of HA in VSMCs. HA calcification of VSMCs was induced by osteogenic factors and a 3D environment. For corroborative visualization of the extent of HA calcification, cells cultured in SM for 4 days were stained with FITC, cHABP, or HABP-19 and observed by fluorescent microscopy. Bright field (top) and fluorescence images (bottom) from mineral layers of VSMCs. HA deposits of VSMCs induced by AA, β-GP, LPC, and 3D-Ns were stained with control (A), FITC (B), cHABP (C) and HABP-19 (D) probes.

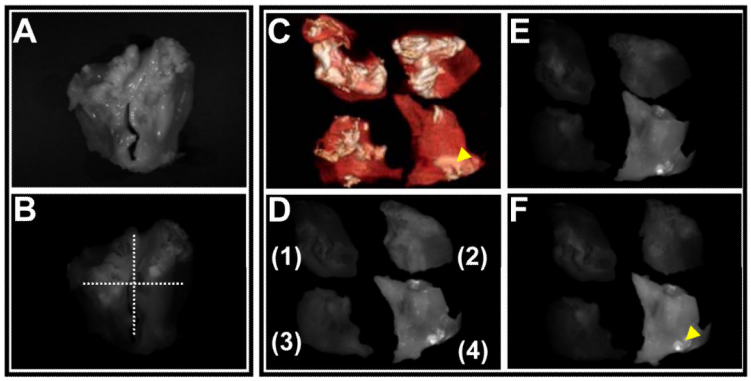

Figure 4.

Ex vivo images of surgically excised aortic valves. (A) Bright field image and (B) fluorescent image of an aortic valve before incubation with probes. The aortic valves were cleaved into four pieces, and then incubated in PBS (control) (1), FITC (2), cHABP-19 (3), or HABP-19 (4) for 1 h, thoroughly washed with PBS to any remove unbound probe from specimen surfaces. μCT imaging (C) was performed at medium resolution and real-time images were reconstructed for correlation with the results of the optical imaging system. White color in the μCT images represents total calcium deposits on the aortic valve surfaces. Cleaved aortic valves were further incubated in PBS for 1 h (D), 8 h (E), and 24 h (F). Optical molecular images were acquired using a Maestro 2 optical imaging system with a 10-ms exposure time. To validate the selective accumulation of imaging probes, a green (FITC) filter set (acquisition setting: 550 to 800 in 10-nm steps) was used. The collected images were delineated as unmixed fluorescence-enhanced signal images (F). The arrowheads in the optical images represent HA deposits on the aortic valve surface.

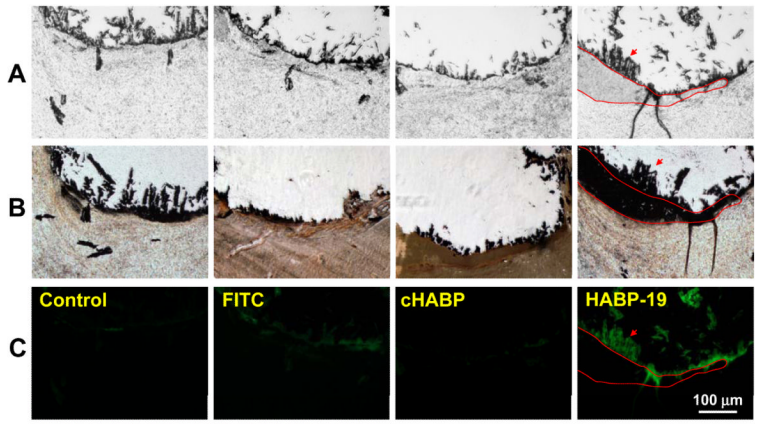

Figure 5.

Histological analysis of aortic valves. (A) Human aortic valves were fixed in paraffin blocks and consecutively sectioned with a 5-μm thickness. The sections were stained with Van Kossa stain (B) or molecular imaging probes (C), including FITC, cHABP, and HABP-19 to detect HA calcification. The red line represents calcium staining by Von Kossa reagents with a black band-like pattern. Staining of consecutive sections by HABP-19 shows restricted HA deposition as indicated by the red arrow.

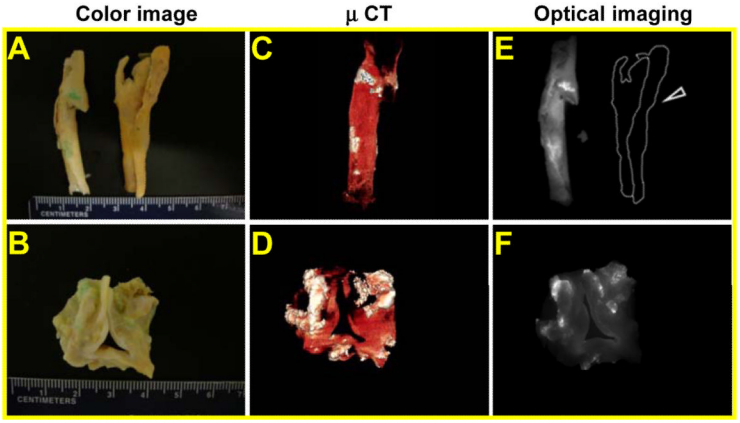

Figure 6.

Ex vivo images of cardiovascular tissues by NIR fluorescence. CEA tissues (A) and aortic valve (B) were incubated with Cy-HABP-19 for 1 h. Digital color images reveal extensive calcification (light cyan) in CEA specimens (A) and aortic valve (B). (C) and (D) μCT images. The white color represents calcified areas on the tissues. (E) and (F) NIR optical fluorescence images. These images are delineated as unmixed fluorescence-enhanced signal images (white) superimposed on the pseudo-background color image (gray). The control sample (marked by a dotted line and open arrowhead in panel C) did not exhibit any noticeable fluorescence in the optical imaging system.

Table 1
Sequences of human OCN template and HABPs

Name	Sequence*
Human OCN	γEPRRγEVCγEL
HABP-19	FITC-βAγEPRRγEVAγELγEPRRγEVAγEL-NH_2
Cy-HABP-19	Cy5.5-CγEPRRγEVAγELγEPRRγEVAγEL-NH_2
cHABP	FITC-βAEPRREVAELEPRREVAEL-NH_2

*HABPs were covalently labeled with FITC or Cy5.5, which was indicated at the N-terminus of each peptide. The Cys of the OCN protein was replaced by Ala (underlined) in the HABPs to avoid complicating disulfide linkages. The bAla of HABP-19 was replaced by Cys to provide a thiol-reactive group for Cy 5.5 dye labeling. γE and βA represent Gla and beta-Ala, respectively.